Catena 172 (2019) 378–386

Contents lists available at ScienceDirect

Catena

journal homepage: www.elsevier.com/locate/catena

PTV-Stream: A simplified particle tracking velocimetry framework for stream surface flow monitoring

Flavia Tauro[a], Rodolfo Piscopia[b], Salvatore Grimaldi[b,c,*]

[a] Centro per l'Innovazione Tecnologica e lo Sviluppo del Territorio, University of Tuscia, Viterbo, Italy
[b] Department for Innovation in Biological, Agro-food and Forest Systems, University of Tuscia, Viterbo, Italy
[c] Department of Mechanical and Aerospace Engineering, Tandon School of Engineering, New York University, Brooklyn, NY, USA

ARTICLE INFO

Keywords:
PTV-Stream
PTV
Surface flow velocity
LSPIV
Image analysis

ABSTRACT

Particle tracking velocimetry (PTV) is a promising image-based approach for remote streamflow measurements in natural environments. However, most PTV approaches require highly-defined round-shaped tracers, which are often difficult to observe outdoors. PTV-Stream offers a versatile alternative to cross-correlation-based PTV by affording the identification and tracking of features of any shape transiting in the field of view. This nearest-neighbor algorithm is inherently thought for estimating surface flow velocity of streams in outdoor conditions. The procedure allows for reconstructing and filtering the trajectories of features that are more likely to pertain to actual objects transiting in the field of view rather than to water reflections. The procedure is computationally efficient and is demonstrated to yield accurate measurements even in case of downsampled image sequences.

1. Introduction

In recent years, an increased attention has been devoted to multi-disciplinarity and innovation in sensing the hydrological cycle (Tauro et al., 2018). Affordable and versatile sensing systems may in fact help mitigate the limitations of traditional measurement stations that currently offer poor spatial coverage but require expensive maintenance (Gleick, 1998; Hannah et al., 2011). Among the new generation of experimental instruments, optical methodologies and image analysis have contributed to advance hydrological observations in several fields. For instance, precipitation, streamflow, and plant water stress are routinely monitored using images (Allamano et al., 2015; Muste et al., 2008; Ludovisi et al., 2017; Abrantes et al., 2018). Integration of optical methods with unmanned aerial vehicle (UAV) technology (Tauro et al., 2015; Perks et al., 2016; Manfreda et al., 2018) and participatory science has also opened up new frontiers in distributed hydrological observations (LeBoursicaud et al., 2015; Le Coz et al., 2016).

Streamflow observations have highly benefitted from optical methods, and the use of image analysis for river monitoring is documented since the 1990s. For instance, large scale particle image velocimetry (LSPIV) is a promising technique that is vastly adopted in hydrology to estimate the surface flow velocity field of water bodies and may be applied to flash flood observation (Jodeau et al., 2008) and to the digital mapping of riverine features (Hauet et al., 2009). Other image-based approaches involve particle tracking velocimetry (PTV) and optical flow that have also been utilized to investigate diverse phenomena spanning from irrigation (Félix-Félix et al., 2017) to volcanic dynamics (Gaudin et al., 2014). Several image-based streamflow studies rely on the installation of permanent and cost-effective gauge-cams in the proximity of the water body of interest to continuously monitor flow dynamics (Bechle et al., 2012; Tauro et al., 2016; Huang et al., 2018). These automated systems comprise digital cameras, controlling units, and, in some cases, laser systems for fully remote photometric calibration. Gauge-cams collect a large volume of images of the water surface that can be off-line analyzed to inspect the streamflow regime at high temporal resolution. However, image-based techniques and gauge-cams are rarely systematically implemented in practical engineering operations probably due to the lack of consistent image processing protocols.

In previous streamflow studies in diverse riverine environments (Tauro et al., 2016; Tauro and Salvatori, 2016; Tauro et al., 2017), correlation-based PTV has been successfully applied to estimate the surface flow velocity field. PTV typically revolves around two phases: particle identification and tracking (Lloyd et al., 1995). In the first phase, images are enhanced to emphasize the appearance of particles in the field of view (for instance, by applying filters and thresholds) and the location of the centroid of the particles in frames is recovered. In the tracking phase, the centroid of the detected particles is identified in subsequent images to reconstruct particle trajectory. Several algorithms have been developed for PTV analysis. In Lloyd et al. (1995), Brevis

* Corresponding author.
E-mail address: salvatore.grimaldi@unitus.it (S. Grimaldi).

https://doi.org/10.1016/j.catena.2018.09.009
Received 8 May 2018; Received in revised form 3 September 2018; Accepted 4 September 2018
Available online 11 September 2018

et al. (2011), cross-correlation is implemented for both particle detection and tracking. In addition, relaxation (Wu and Pairman, 1995), heuristics based on a priori knowledge of the flow (Tang et al., 2008), and Voronoï tracking scheme (Aleixo et al., 2011) have also been utilized. Upon PTV processing, particle trajectories are reconstructed based on velocity vectors that are randomly located in the field of view. Surface flow velocity maps can be generated by interpolating particle trajectories.

PTV presents several advantages with respect to alternative approaches. Firstly, it allows for identifying and reconstructing the trajectory of individual features transiting in the field of view, thus tangibly relating velocity estimations to physical objects. By imposing conditions on the trajectories, see for instance Hassan and Canaan (1991), Tauro et al. (2017), velocity measurement accuracy can be considerably improved. Further, PTV does not involve spatial averaging and can be successfully adopted in case of velocity gradients (Fuchs et al., 2017).

PTV is designed for low seeding density flows and does not require assumptions on flow steadiness nor on the relative position of neighbor particles. Its applications in hydrological sciences are diverse and involve dispersion in porous media (Moroni and Cushman, 2001), exchange processes between rivers and groynes (Uijttewaal et al., 2001; Yossef and deVriend, 2011) and tidal patterns (Kimura et al., 2011), and sediment transport (Radice et al., 2017; Ballio et al., 2018). In most algorithms, PTV is dependent on the presence of tracers whose shape is a priori known. Such a feature has considerably limited the implementation of PTV in outdoor experimental studies where the controlled deployment of particles may be challenging. In fact, the instance of naturally occurring round features is rare, and deploying a large amount of particles in difficult to access riverine environments can be impractical. On the other hand, the alternative LSPIV approach has been extensively applied (Fujita et al., 1997). This technique applies the principles of classical Particle Image Velocimetry (PIV) (Adrian, 1991, 2005; Raffel et al., 2007; Peterson et al., 2008) to recognize and track patterns on the water surface of natural streams, and may be applied also without deploying objects in the current (Tauro et al., 2017). For a comparison between LSPIV and PTV, refer to Tauro et al. (2017).

Experimental PTV applications entail: i) definition and imaging of the field of view; ii) orthorectifying images through transformation schemes that rely on the known coordinates of a minimum of six ground control points (GCPs; in this phase, photometric calibration and camera lens distortion removal may also occur); and iii) image processing. In Tauro et al. (2014), image orthorectification and GCPs surveying are prevented by maintaining the camera optical axis perpendicular to the field of view and by utilizing medium-power lasers to create reference points at known distance in images, thus enabling fully remote photometric calibration.

In this work, we propose a novel simple PTV approach, PTV-Stream, specifically aimed at estimating the surface flow velocity of natural water bodies in outdoor conditions. The procedure functions as a nearest-neighbor algorithm, whereby low seeding density is assumed in the field of view. Tracers of any shapes can be identified and tracked in images based on their luminance with respect to the background. The algorithm requires a priori known direction of the flow average velocity that should be approximately perpendicular to the cross section, and allows for reconstructing and filtering tracer trajectories that are more likely to pertain to actual objects transiting in the field of view rather than to water reflections. The procedure is developed in Java and offers a computationally efficient alternative to correlation-based PTV schemes. In this study, we apply PTV-Stream to experimentally controlled videos taken on the Brenta River and to a video of a moderate flood in the Tiber River. We compare our PTV-Stream findings to the cross-correlation-based PTV procedure developed by Brevis et al. (2011) and implemented in Tauro et al. (2017) (correlation-based PTV in the rest of this manuscript) and to independent benchmark data collected with a current meter or with radar technology.

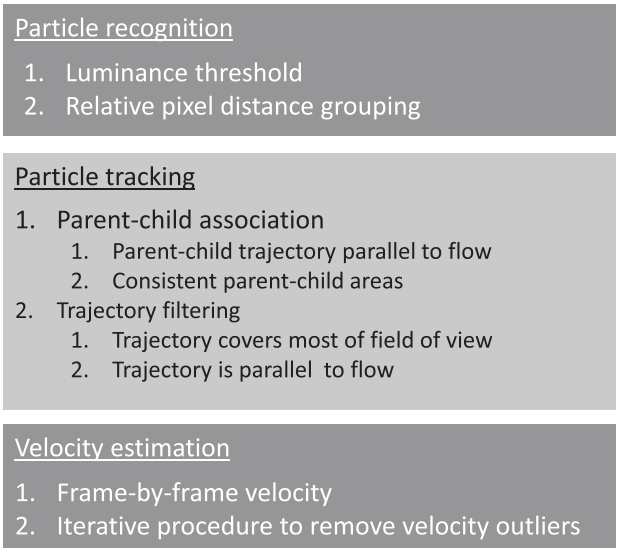

Fig. 1. Flowchart of PTV-Stream.

2. PTV-Stream

PTV-Stream is a particle tracking procedure that aims at identifying the trajectories of objects floating on the stream surface and passing through the field of view. The method can be applied on a sequence of images recorded at a fixed acquisition frequency with an RGB camera. The outputs of the procedure include the objects' trajectories and velocities in pixels per frame. The metric dimension of pixels must be independently estimated to obtain output velocities in meters per second. The sequence of images may be obtained from video captured with permanent cameras, mobile setups, and aerial platforms. Photometric calibration may be attained by a priori determining the camera intrinsic parameters and through camera geometric calibration in laboratory conditions. Alternatively, similar to Tauro et al. (2016, 2014), the system of low power lasers may be used.

PTV-Stream is organized in three main phases: particle recognition, particle tracking, and velocity estimation, see Fig. 1. Different from traditional PTV approaches, PTV-Stream does not involve interpolation of results. Rather, trajectory-based average velocities are computed in the region of interest. This is related to the fact that homogeneously and densely seeded water surfaces are rarely encountered in field settings. Therefore, interpolating sparse instantaneous velocities may result in significant uncertainty. Towards a correct implementation of the algorithm, it is assumed that the camera field of view is directed with its width along the river cross-section and that the height of the field of view is approximately orthogonal to the cross-section. Further, particles are assumed to follow the stream average flow direction and, therefore, their trajectories should be fairly orthogonal to the river cross-section. These simple assumptions are consistent with previous work by Hassan and Canaan (1991) and can be easily verified by properly orienting the camera in the experimental setup or rotating captured images. It is also advisable to preliminarily take a look at experimental videos to roughly determine the average dimension of the tracers transiting in the field of view, their luminance in varying illumination conditions, and the average frame-to-frame pixel displacement.

The particle recognition phase is an appearance-based method that detects objects based on their luminance without searching for specific geometric shapes. Object detection is directly conducted on RGB images. Specifically, since floating material can be lighter or darker than the background, in the experiments, we arbitrarily choose to track light tracers and discard dark ones, even though the opposite choice is also possible. Therefore, all pixels whose luminance is higher than a certain threshold value are regarded as pertaining to a potential

particle. It is indeed assumed that particles exhibit a higher luminance with respect to the image background. Higher luminance pixels are then grouped based on their relative distance. Such distance value can be selected through a preliminary inspection of the image sequence, and is related to the pixel dimensions of the tracers. For instance, if a tracer can be enclosed in a circle of 10 pixels of diameter, the distance threshold can be set to 10. Once a tracer is identified, the pixel coordinates of its centroid and its area are computed. Tracers whose area is below a certain value (determined by the user) are rejected and are not accounted for in the successive tracking phase. Such a constraint contributes to limit computational times.

The tracking phase works as follows. Each identified tracer in the first frame is regarded as a parent of a child tracer in the successive frame. The association of parent to child tracers is performed by imposing the following conditions on their metrics. Firstly, the tracer should follow the stream average flow and, therefore,

$$\arctan\frac{(\boldsymbol{X}_i-\boldsymbol{X}_{i\text{-}1})\cdot\boldsymbol{j}}{(\boldsymbol{X}_i-\boldsymbol{X}_{i\text{-}1})\cdot\boldsymbol{i}}>\frac{\pi}{4} \tag{1}$$

whereby, $\boldsymbol{X}_i$ and $\boldsymbol{X}_{i\text{-}1}$ are the position vectors of the child and parent tracer centroids and $\boldsymbol{j}$ and $\boldsymbol{i}$ are unit vectors oriented parallel and perpendicular to the flow (that is, they are aligned to the frame height and width), respectively. Eq. (1) is valid in case of right-wise deviations of the average flow direction with respect to the image height. For left-wise deviations, the equation should be modified to $\pi-\arctan\frac{(\boldsymbol{X}_i-\boldsymbol{X}_{i\text{-}1})\cdot\boldsymbol{j}}{(\boldsymbol{X}_i-\boldsymbol{X}_{i\text{-}1})\cdot\boldsymbol{i}}>\frac{\pi}{4}$. Secondly, the parent and child tracers' areas should not sensibly change between successive frames. Such a constraint can be verified by imposing that parent and child areas should not differ by more than a threshold percentage (typically, child areas should not be less than 20% or larger than 120% of parent areas). Finally, the child tracer should lay within a rectangular search area whose vertex is the centroid of the parent tracer. This can be implemented by conducting the tracking procedure within a search area of dimensions imposed by the users and has the beneficial effect of considerably reducing time for computation. If more than a child tracer satisfies the above conditions, the child tracer closest to the parent position is selected.

The tracking procedure can be implemented on an entire sequence of frames. As the computation proceeds, the coordinates of parent and child tracers are stored. Tracking conditions are not verified if a parent tracer cannot be associated to a child. This may occur due to sudden variations in illumination conditions or to submersion effects. In this case, the eventual instance of the child tracer is verified by computing the tracking conditions on a number of successive frames selected by the user.

In case of highly agglomerated tracers, it may be possible to observe an object that separates into several other shapes in successive frames. When processed with PTV-Stream, such frames may lead to child tracers having no parent particles in previous frames. In similar cases, the algorithm treats the unassociated child tracer as a parent for the successive frame.

Once the tracking has been implemented on all frames of the sequence, parent and child tracer coordinates are saved and trajectories can be plotted. A filtering procedure is then implemented on the tracer trajectories as in Tauro et al. (2017). Specifically, velocities are computed from trajectories that cover a significant region of the field of view and that minimally deviate from the average flow direction. Such conditions are imposed by setting

$$\|\boldsymbol{X}_{end}-\boldsymbol{X}_{start}\|>\frac{1}{5}H. \tag{2}$$

whereby H is the image height, and $\boldsymbol{X}_{end}$ and $\boldsymbol{X}_{start}$ indicate the tracer position vectors in the final and first images of the trajectory, respectively. Further, the orientation of the trajectory is validated through

$$\arctan\left[\frac{(\boldsymbol{X}_{end}-\boldsymbol{X}_{start})\cdot\boldsymbol{j}}{(\boldsymbol{X}_{end}-\boldsymbol{X}_{start})\cdot\boldsymbol{i}}\right]>\frac{4}{9}\pi \tag{3}$$

for right-wise deviation. In case of left-wise deviations, Eq. (3) should be modified to $\pi-\arctan\left[\frac{(\boldsymbol{X}_{end}-\boldsymbol{X}_{start})\cdot\boldsymbol{j}}{(\boldsymbol{X}_{end}-\boldsymbol{X}_{start})\cdot\boldsymbol{i}}\right]>\frac{4}{9}\pi$. These conditions aim at retaining reliable trajectories of similar duration (Eq.(2)) and oriented along the average flow direction.

The trajectory-based velocity is determined by first computing instantaneous velocities along the same trajectory and then calculating their average. Specifically, for a consistent trajectory, instantaneous surface streamflow velocity between successive frames, $V_{i\text{-}1/2}$, is then determined as

$$V_{i\text{-}1/2}=\frac{\|\boldsymbol{X}_i-\boldsymbol{X}_{i\text{-}1}\|}{\Delta t_i} \tag{4}$$

where Δt_i is the time interval between two successive frames. To remove eventual velocity outliers, an iterative procedure is implemented on the computed $V_{i\text{-}1/2}$. Specifically, the trajectory-based average velocity, $\hat{V}$, and standard deviation, $\hat{\sigma}$, are calculated over the series of $V_{i\text{-}1/2}$ of a consistent trajectory. If the condition $V_{i\text{-}1/2}\in(\hat{V}-5\hat{\sigma},\ \hat{V}+5\hat{\sigma})$ is not verified for a generic $V_{i\text{-}1/2}$ value, then, such a value is cancelled and the condition again computed until only frame-by-frame velocities laying in the selected confidence interval are retained.

PTV-Stream is effective at recognizing features of diverse shapes in images. Here, we report some examples of object recognition for non-round features. In Fig. 2, two frames recorded at the permanent gauge-cam station on the Tiber River (Tauro et al., 2016) on March, 5th, 2015 at 20:00 are displayed. In Fig. 2 (a), among various features, a plastic irregular object and a wood stick are identified by the algorithm. The inset in (a) shows a close-up of the detected objects and their

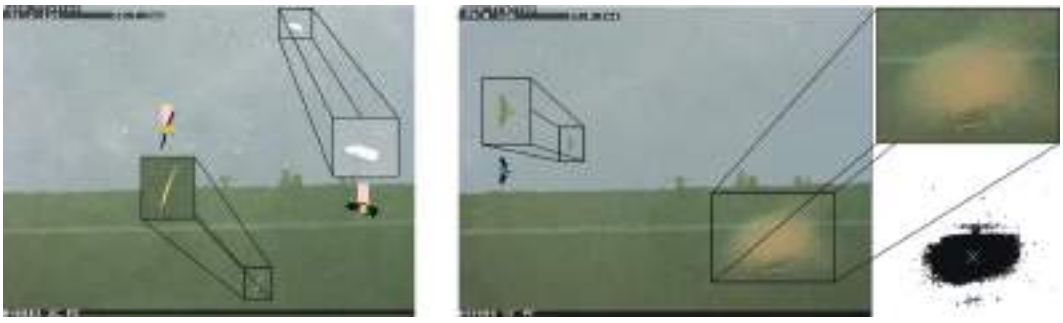

(a) (b)

Fig. 2. Snapshots recorded at the permanent gauge-cam station on the Tiber River (Tauro et al., 2016) on March 5th, 2015 at 20:00 depicting (a) a plastic irregular object and a wood stick and (b) a flying bird and a brownish spot. The insets display close-up views of the recognized objects.

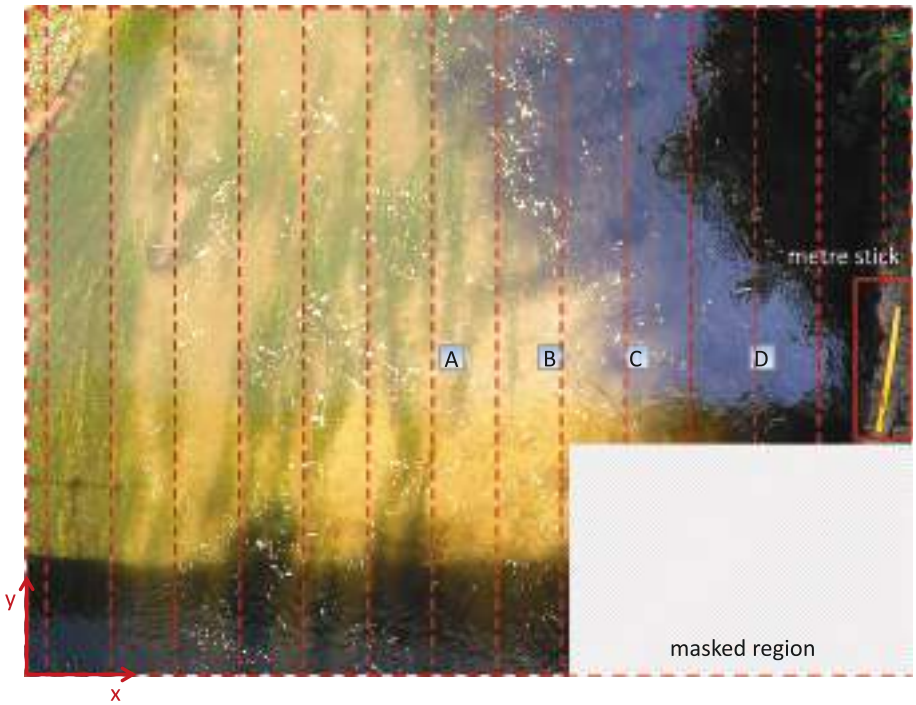

Fig. 3. Representative processed image depicting the field of view on the Brenta River, locations of the current meter measurements (A to D), and vertical regions used for comparing velocities.

Table 1
Average benchmark velocities ($\bar{v}_b$) and standard deviations (σ_b) measured with the current meter at locations illustrated in Fig. 3.

	A	B	C	D
$\bar{v}_b$ [m/s]	0.46	0.45	0.31	0.32
σ_b [m/s]	0.04	0.03	0.02	0.02

appearance upon applying an RGB threshold. The yellow dot indicates the position of the object centroid and the pink rectangle the search window for parent-child association. In Fig. 2 (b), two detected features are not considered for the tracking procedure. Specifically, the algorithm identifies the reflection of a bird flying above the stream; however, due to its trajectory, the shadow is not further considered for the tracking phase. Also, a brownish spot is initially detected as a candidate tracer but it rapidly disappears in subsequent frames. The wood stick below the brownish spot is not entirely buoyant and, therefore, its visible portions are regarded as tracers. However, the luminance and area of such smaller portions do not satisfy the constraints for tracking analysis.

3. Comparison analysis

The efficacy of PTV-Stream to estimate surface flow velocity is demonstrated by analyzing a dataset previously studied with LSPIV and correlation-based PTV (Tauro et al., 2017). Specifically, correlation-based PTV was implemented by adopting a command-line version of PTVLab (Brevis et al., 2011) and then filtering the obtained trajectories with the constraints in Eqs. (2) and (3). An additional constraint was also imposed on the angle between the positions of parent and child tracers in successive images (see Eq. (1) in Tauro et al. (2017)). Such a condition aimed at discarding trajectory jumps due to particle agglomerates.

The set of data was collected on the Brenta River in Northern Italy in 2015. Therein, care was taken to continuously and homogeneously deploy woodchips in the field of view. Based on the work in Tauro et al. (2017), correlation-based PTV generally led to velocity estimations in closer agreement with benchmark data obtained from independent traditional measurement equipment such as current meters and radars, than well-established LSPIV. Herein, we report velocity estimations obtained with PTV-Stream and compare them to results gathered with previous correlation-based PTV analyses.

3.1. Brenta River: study site and materials

The experiment was conducted on June 10th, 2015 at 46°02′20.8122″ North Latitude, 11°24′37.3349″ East Longitude, 464.38 elevation in the WGS84 coordinate system. Videos were recorded with the telescopic portable apparatus introduced in Tauro et al. (2014), featuring a GoPro Hero 4 Black edition camera with its optical axis orthogonal to the water surface, thus preventing image orthorectification. Photometric calibration was enabled by a meter-stick placed on the right-side stream bank at the same level of the water surface. The field of view captured a horizontal area of 9.5 × 5.3 m^2. A full HD (1920 × 1080 pixels) RGB video was captured at 50 Hz and then segmented into 12 video sequences of 20 s each. The image sequences were subsampled at 25 Hz and the field of view was trimmed to 1430 × 1080 pixels. The bottom right corner of the images displayed vegetation leaning from the bridge and, to prevent disturbances in velocity estimation due to vegetation motion, an area of 552 × 375 pixels was masked with a black patch. The fish-eye lens distortion was removed using the open-source software GoPro Studio.

Benchmark velocity measurements were conducted with the OTT Hydromet C2 current meter at 3 cm below the water surface at four locations along the stream cross-section up to 3.5 m from the right-side river bank (A to D in Fig. 3). Additional acquisitions on the left-side river bank were challenging due to the presence of vegetation in the stream. Twelve replicates were performed at each location; average velocities ($\bar{v}_b$) and standard deviations (σ_b) are reported in Table 1. On average, surface flow velocity was estimated to be slightly less than 0.4 m/s.

Correlation-based PTV was executed using a modified version of PTVLab (Brevis et al., 2011). The algorithm includes particle detection

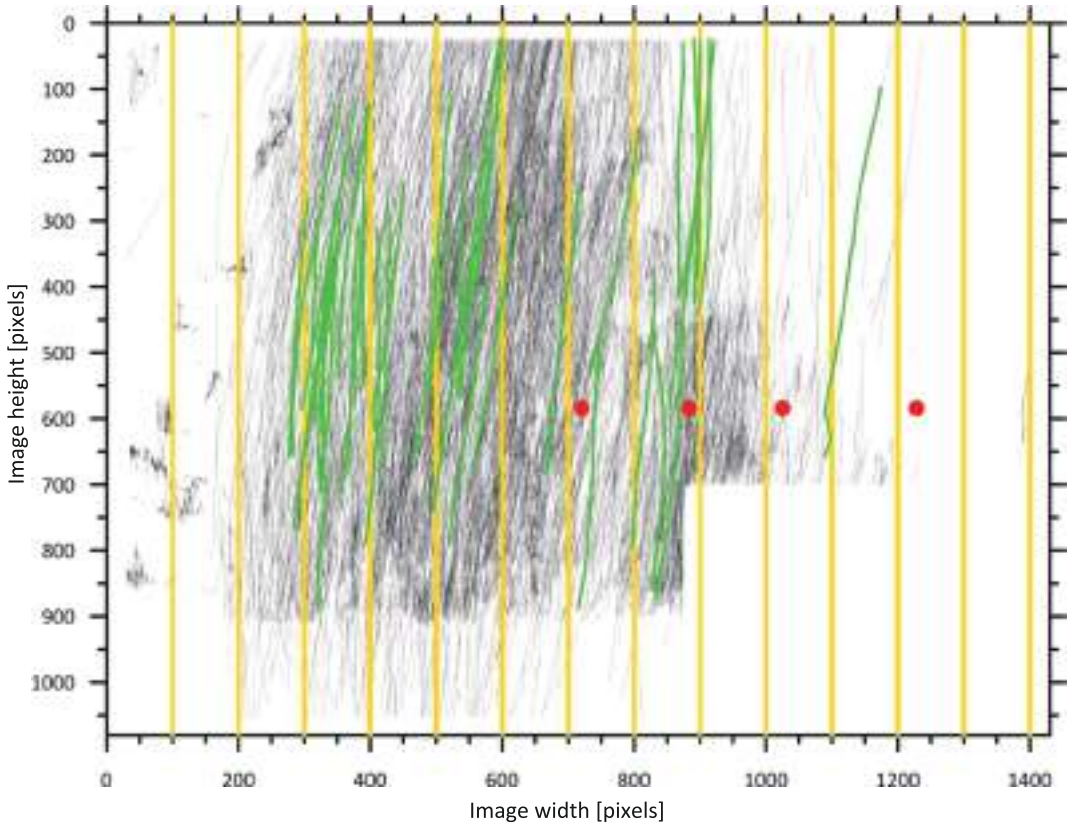

Fig. 4. Representative map of the trajectories obtained with PTV-Stream on one of the image sequences of the Brenta River. Black lines are the identified trajectories, green lines are the filtered trajectories, and red circles are locations of the measurements taken with the current meter. Yellow vertical lines refer to the vertical regions of the field of view.

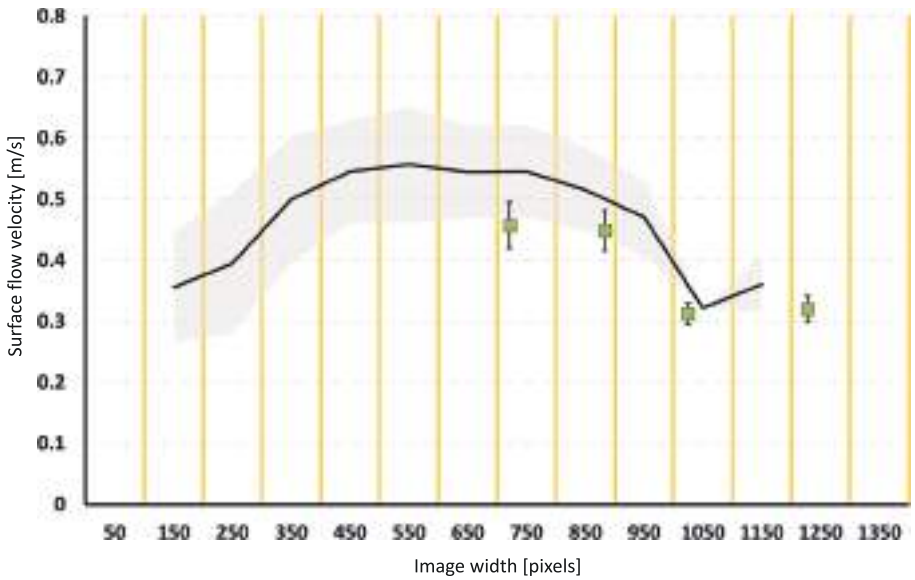

Fig. 5. Comparison of the cross-sectional velocities (black line) obtained on the Brenta River with PTV-Stream to benchmark measurements (green squares). The shaded gray area indicates the standard deviation of velocities obtained with PTV-Stream. Yellow vertical lines refer to the vertical regions of the field of view.

via thresholding and cross-correlation with a symmetric Gaussian kernel thus, the image intensity threshold, the standard deviation of the Gaussian distribution, and the correlation cutoff threshold were set to 130, 12 pixels, and 0.5, respectively. Particle tracking was implemented using cross-correlation by interrogation area. The size of the square interrogation area, the cross-correlation cutoff threshold, and the similarity percentage among neighbor particles were set to 20 pixels, 0.4, and 20%, respectively. Further details can be found in Tauro et al. (2017). To compare velocity estimations obtained with PTV-Stream, correlation-based PTV, and the current meter, the field of view was divided into vertical regions. Such regions were selected to be homogeneous in width. For each vertical region, velocity estimations were computed according to the procedure in Section 2. Further, to offer a comprehensive comparison, the velocities obtained in each vertical

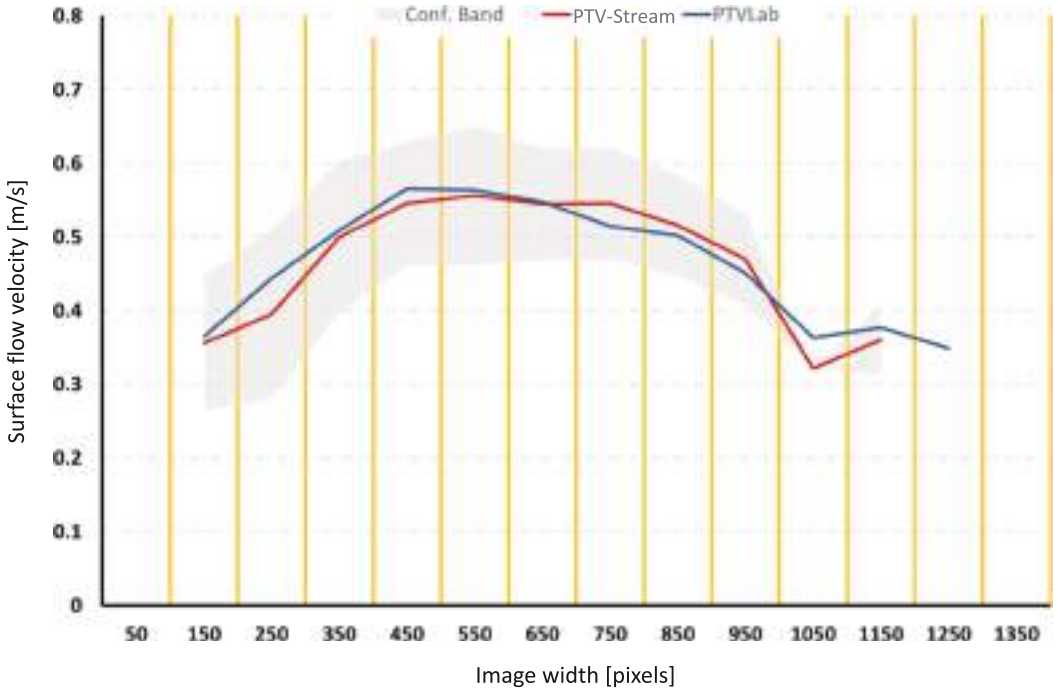

Fig. 6. Comparison of the cross-sectional velocities obtained on the Brenta River with PTV-Stream (red line) to correlation-based PTV performed with PTVLab (blue line). The shaded gray area indicates the standard deviation of velocities obtained with PTV-Stream. Yellow vertical lines refer to the vertical regions of the field of view.

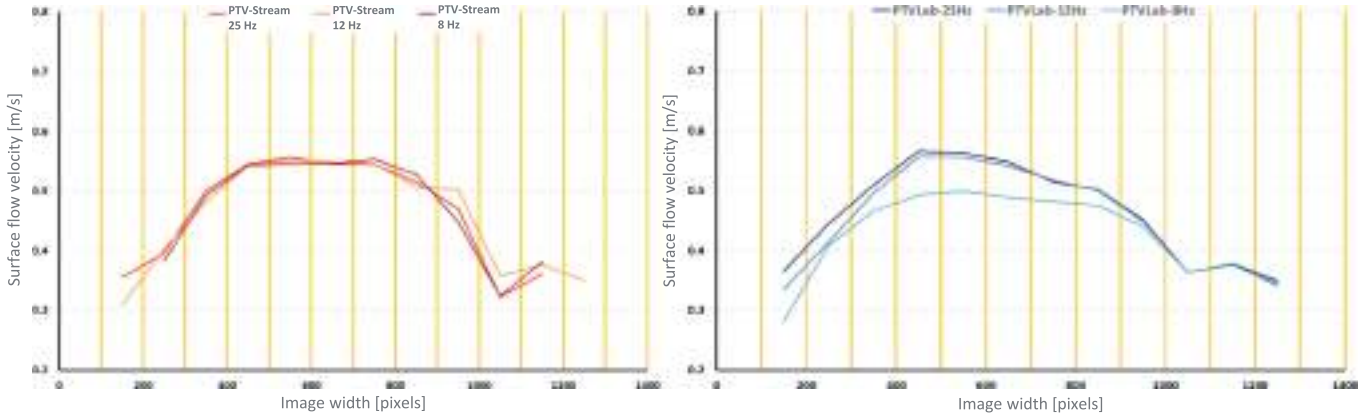

Fig. 7. Average cross-sectional velocity profiles obtained for image sequences of the Brenta River processed with PTV-Stream (left) and PTVLab (right) sampled at 25 Hz, 12 Hz, and 8 Hz.

region for each image sequence were averaged and their mean values and standard deviation computed. Such values were then compared to benchmark measurements performed at locations A to D.

3.2. PTV analysis and velocity data comparison

Fig. 4 depicts a representative map obtained with PTV-Stream for one of the image sequences. All the identified trajectories are illustrated in black, whereas filtered ones are in green. All of the trajectories pertain to features actually transited in the field of view. The amount of green trajectories may be increased based on the user's judgment in setting less severe constraints on the orientation or the minimum length of the trajectory.

In Fig. 5, velocities (bold black line) and standard deviations (shaded gray areas) obtained with PTV-Stream are compared to benchmark values (green squares) and their standard deviations. PTV-Stream results correctly capture the higher velocity in the center of the stream cross-section and are in agreement with benchmark data. PTV-Stream data are generally slightly higher than benchmark measures: the mean cross-sectional value is equal to 0.46 m/s, whereas the benchmark cross-sectional mean equals 0.38 m/s. Standard deviations are also larger for PTV-Stream data (on average equal to 7.5 cm/s) than for benchmark measurements (on average equal to 2.8 cm/s). Such slight differences are attributed to the fact that image-based measurements are relative to the stream water surface, whereas current meter-based data are executed at a few centimeters below the water surface.

In Fig. 6, cross-sectional velocity profiles obtained with PTV-Stream and PTVLab are compared. The profiles are mostly overlapped, thus confirming the efficacy of PTV-Stream with respect to correlation-based PTV. Remarkably, PTV-Stream is coded in a fully scalable java TM implementation, which takes advantage of CPU power multithreading and considerably reduces computational times with respect to PTVLab (on average, on the same computer, PTV-Stream takes 17 min with a deviation of 7 min to analyze a video, whereas PTVLab takes 162 min with a deviation of 18 min). Also, PTV-Stream runtime can be further decreased by subsampling the video acquisition frequency. For

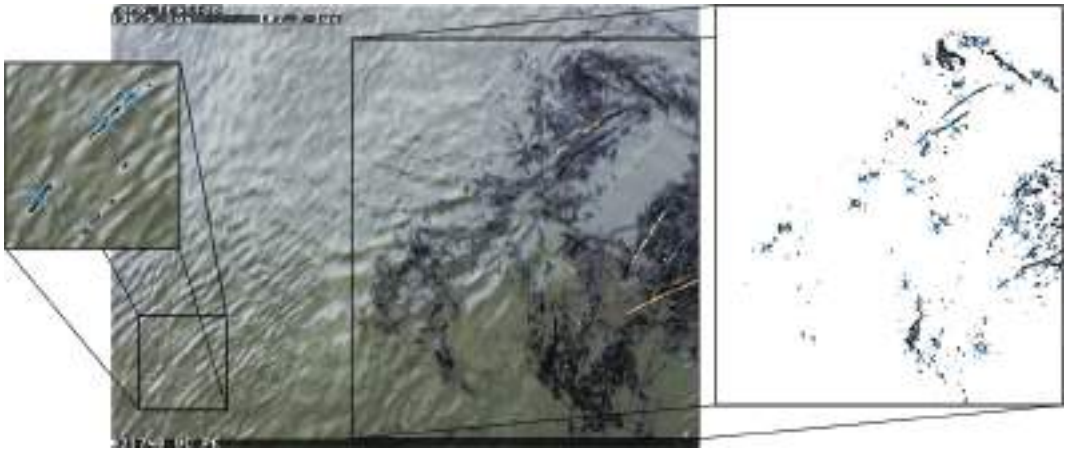

Fig. 8. Snapshot recorded at the permanent gauge-cam station on the Tiber River (Tauro et al., 2016) on February 6th, 2015, at 7:40 illustrating water ripples. The inset displays a close-up view of the recognized objects.

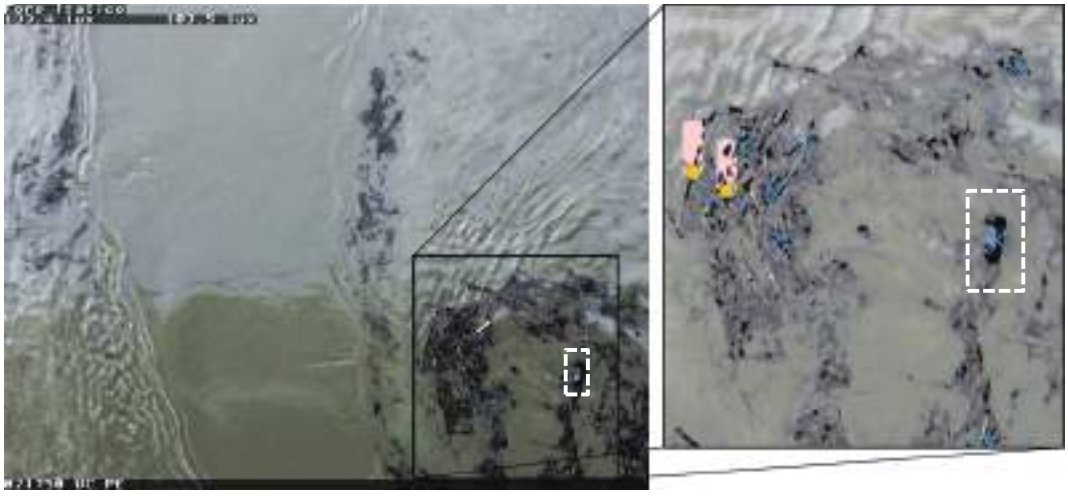

Fig. 9. Snapshot recorded at the permanent gauge-cam station on the Tiber River (Tauro et al., 2016) on February 6th, 2015, at 7:40 illustrating debris, a plastic bottle (enclosed in the dashed white rectangle), and wood sticks. The inset displays a close-up view of the recognized objects.

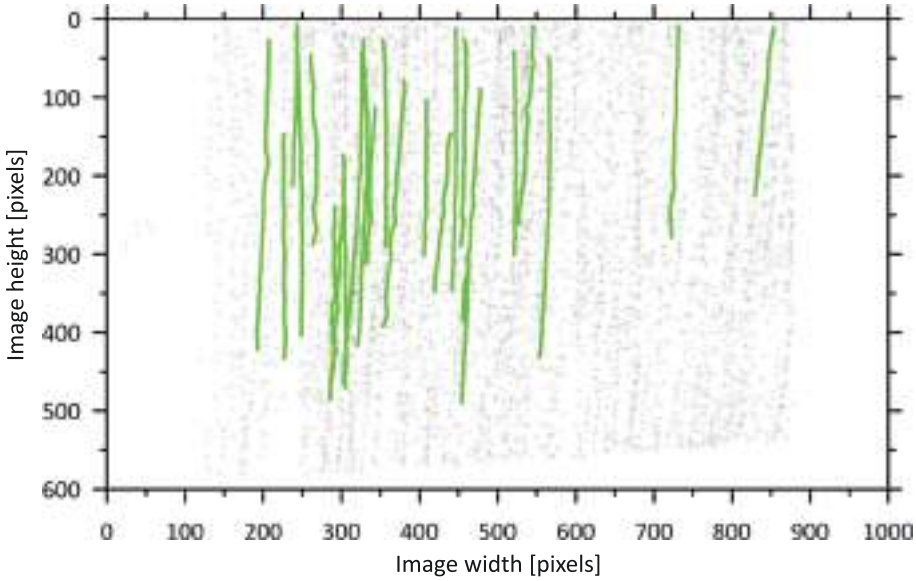

Fig. 10. Map of the trajectories obtained with PTV-Stream on the image sequences of the Tiber River. Black lines are the identified trajectories and green lines are the filtered trajectories.

instance, in Fig. 7 (left), PTV-Stream velocity data are reported for the image sequences of the Brenta River sampled at 25 Hz, 12 Hz, and 8 Hz. The cross-sectional profiles are largely overlapped, thus supporting the robustness of the procedure. On the other hand, in Fig. 7 (right), PTVLab results for similar acquisition frequencies exhibit larger variability. Specifically, if a frequency of 8 Hz is selected, the velocity at the center of the stream sensibly decreases. Regarding computational times, it is noted that PTV-Stream Matlab implementation (a beta version is freely available upon request) is also more efficient than PTVLab. In fact, by circumventing the need for computationally expensive cross-correlation, the procedure runtime is improved.

4. Future challenges

The potential of PTV-Stream is foreseen to aid hydrological monitoring in challenging settings, such as, for instance, floods and high flow regime, whereby the use of traditional equipment may be hampered. Herein, we report a comparative analysis of a set of data taken during a moderate flood at the gauge-cam station on the Tiber River in 2015. Naturally occurring features were exclusively present in the field of view; however, the presence of dishomogeneous objects (agglomerated debris) and the mirror-like river surface posit severe challenges to image-based analysis. In particular, neither LSPIV nor correlation-based PTV led to accurate results.

Images on the Tiber River were captured on February 6th, 2015, through the gauge-cam station described in Tauro et al. (2016), Tauro and Salvatori (2016). The gauge-cam station enables the acquisition of one-minute long videos every ten minutes through a Mobotix FlexMount S15 weatherproof internet protocol camera. Only images captured with the right-side L25 lens (82° angle of view and 4 mm focal length) were analyzed since they depicted a larger field of view (16.15×12.11 m^2). The gauge-cam consists of a MOBOTIX S15 camera with its optical axis perpendicular to the water surface that minimizes distortions and circumvents orthorectification. Photometric calibration is enabled by a system of two < 20 mW green (532 nm wavelength) lasers installed at 50 cm on both sides of the camera. The lasers are activated for 20 s at the beginning of each video, and generate highly visible reference points located 1 m apart on the water surface. The frame acquisition frequency of the gauge-cam station is automatically adjusted based on external illumination conditions and, thus, varies for each captured clip. Further, each one-minute long video is saved as numerous highly-compressed and reduced-size clip files (where the number of clips depends on the size of the video and, in turn, on the acquisition frequency).

Consistent with Tauro et al. (2017), a one-minute video captured during the flood peak at 7:40 was analyzed. During the video, the nearby RVM20 speed surface radar recorded an average surface velocity of 2.33 m/s. During the flood, debris and diverse objects transited in the field of view, therefore, tracer deployment was unnecessary. The selected video was saved as nine different clips whose duration and acquisition frequency ranged within 4 to 8 s and from 4 to 8.72 Hz, respectively. The analyzed sequence was obtained by decompressing each clip and the overall frequency was estimated to 6.95 Hz as a weighted average of each clip's frequency. Image resolution was 1024×768 pixels and images of the flood on the Tiber River were affected by barrel distortion due to the wide-angle L25 lens. Fisheye distortion was removed using the Adobe Photoshop “Lens correction” filter.

Feature detection with PTV-Stream presented several criticalities. Figs. 8 and 9 depict two snapshots captured during the flood. Fig. 8 displays several ripples with high luminance variability. The area of such features varies significantly and, therefore, they were not taken into account as tracers. In Fig. 9, a large amount of debris and plastic objects transits in the bottom right of the field of view. In this case, the debris was discarded since it is below the luminance threshold. A floating bottle is recognized but its frame-by-frame displacement exceeds the dimension of the search window and was thus not tracked. Once the bottle is farther from the bottom of the field of view (where bridge piers are located), its velocity decreases and was then tracked by the algorithm. The bright wood sticks on the left of the close-up were instead successfully recognized and tracked.

Fig. 10 depicts the trajectories identified (black lines) and retained (green lines) for velocity estimation. In spite of the challenging experimental conditions, PTV-Stream successfully identified several trajectories. The average surface flow velocity computed based on the green trajectories is equal to 1.60 m/s and the standard deviation to 0.09 m/s. This value is higher than the results obtained with PTVLab (1.4 m/s) but still significantly lower than radar velocity (2.33 m/s). This fact is attributed to the severe appearance of the water surface (mirror-like surface with large agglomerated objects transiting in the field of view) that may negatively affect parent-child association during tracking. Also, due to the irregular frame acquisition frequency of the gauge-cam, objects sensibly change their velocity in the field of view and, therefore, the selection of the size of the rectangular search area is challenging. Despite such criticalities, the performance of PTV-Stream is slightly better than traditional PTV and LSPIV, and we expect the algorithm to lead to improved estimations in case of fixed frame acquisition frequencies.

Another significant challenge entails the implementation of PTV-Stream for streamflow rate measurements and the development of rating curves. Though this is still a poorly explored field, PTV-Stream is expected to beneficially contribute to the noninvasive observation of flow rate by providing accurate and distributed estimation of surface flow velocity. Accurate surface flow kinematics description may be complemented with the methodology by Chiu (1991), Moramarco et al. (2004) to obtain the mean velocity and, thus, flow rate.

5. Conclusions

PTV-Stream is a simplified particle tracking velocimetry approach to estimate the surface flow velocity of natural water bodies. The procedure is a nearest-neighbor algorithm that allows for identifying and tracking features of any shape, such as the ones naturally occurring in streams. Tested on several artificially-seeded videos of the Brenta River, Italy, the algorithm is in good agreement with correlation-based PTV and benchmark measurements. Computational times are more efficient than correlation-based PTV and the algorithm is relatively unaffected if images are subsampled down to a frame frequency of 8 Hz. Experimental findings on the video of a moderate flood on the Tiber River are less satisfactory due to the particularly adverse appearance of the water surface and to irregular frame frequency. Nonetheless, results are in higher agreement with benchmark radar data than traditional PTV.

This simple yet computationally efficient procedure may be a valid alternative to more established methodologies for outdoor hydrological observations. In particular, the method is robust even at low image acquisition frequencies and could be easily implemented in gauge-cams for the real-time analysis of streamflow regime. Future efforts will be devoted to the analysis of large gauge-cam-based datasets for fine-tuning and enhancement of the methodology, and to image-based estimation of flow rate.

Acknowledgments

This work was supported by POR-FESR 2014-2020 n. 737616 INFRASAFE, by the UNESCO Chair in Water Resources Management and Culture, and by Fondi ricerca scientifica di Ateneo - Linea B 2016 from University of Tuscia. Declarations of interest: none.

References

Abrantes, J.R.C.B., Moruzzi, R.B., Silveira, A., deLima, J.L.M.P., 2018. Comparison of

thermal, salt and dye tracing to estimate shallow flow velocities: novel triple-tracer approach. J. Hydrol. 557, 362–377.
Adrian, R.J., 1991. Particle-imaging techniques for experimental fluid-mechanics. Annu. Rev. Fluid Mech. 23, 261–304.
Adrian, R.J., 2005. Twenty years of particle image velocimetry. Exp. Fluids 39 (2), 159–169.
Aleixo, R., Soares-Frazão, S., Zech, Y., 2011. Velocity-field measurements in a dam-break flow using a PTV Voronoï imaging technique. Exp. Fluids 50 (6), 1633–1649.
Allamano, P., Croci, A., Laio, F., 2015. Toward the camera rain gauge. Water Resour. Res. 51 (3), 1744–1757.
Ballio, F., Pokrajac, D., Radice, A., Sadabadi, S.A.H., 2018. Lagrangian and Eulerian description of bed load transport. J. Geophys. Res. Earth Surf. 123 (2), 384–408.
Bechle, A., Wu, C., Liu, W., Kimura, N., 2012. Development and application of an automated river-estuary discharge imaging system. J. Hydraul. Eng. 138 (4), 327–339.
Brevis, W., Niño, Y., Jirka, G.H., 2011. Integrating cross-correlation and relaxation algorithms for particle tracking velocimetry. Exp. Fluids 50 (1), 135–147.
Chiu, C.L., 1991. Application of entropy concept in open-channel flow study. J. Hydraul. Eng. 117 (5), 615–628.
Félix-Félix, J.R., Salinas-Tapia, H., Bautista-Capetillo, C., García-Aragón, J., Burguete, J., Playán, E., 2017. A modified particle tracking velocimetry technique to characterize sprinkler irrigation drops. Irrig. Sci. 35 (6), 515–531.
Fuchs, T., Hain, R., Kähler, C.J., 2017. Non-iterative double-frame 2D/3D particle tracking velocimetry. Exp. Fluids 58 (119), 1–5.
Fujita, I., Muste, M., Kruger, A., 1997. Large-scale particle image velocimetry for flow analysis in hydraulic engineering applications. J. Hydraul. Res. 36 (3), 397–414.
Gaudin, D., Taddeucci, J., Scarlato, P., Moroni, M., Freda, C., Gaeta, M., Palladino, D.M., 2014. Pyroclast tracking velocimetry illuminates bomb ejection and explosion dynamics at Stromboli (Italy) and Yasur (Vanuatu) volcanoes. J. Geophys. Res. Solid Earth 119 (7), 5384–5397.
Gleick, P.H., 1998. Water in crisis: paths to sustainable water use. Ecol. Appl. 8 (3), 571–579.
Hannah, D.M., Demuth, S., van Lanen, H.A.J., Looser, U., Prudhomme, C., Rees, G., Stahl, K., Tallaksen, L.M., 2011. Large-scale river flow archives: importance, current status and future needs. Hydrol. Process. 25 (7), 1191–1200.
Hassan, Y.A., Canaan, R.E., 1991. Full-field bubbly flow velocity measurements using a multiframe particle tracking technique. Exp. Fluids 12 (1), 49–60.
Hauet, A., Muste, M., Ho, H.C., 2009. Digital mapping of riverine waterway hydrodynamic and geomorphic features. Earth Surf. Process. Landf. 34 (2), 242–252.
Huang, W.C., Young, C.C., Liu, W.C., 2018. Application of an automated discharge imaging system and LSPIV during typhoon events in Taiwan. Water 10 (3), 280.
Jodeau, M., Hauet, A., Paquier, A., Le Coz, J., Dramais, G., 2008. Application and evaluation of LS-PIV technique for the monitoring of river surface velocities in high flow conditions. Flow Meas. Instrum. 19 (2), 117–127.
Kimura, N., Liu, W.C., Wu, C.H., Bechle, A.J., Chen, W.B., Huang, W.C., 2011. Flow measurement with multi-instrumentation in a tidal-affected river. Water Environ. J. 25 (4), 563–572.
Le Coz, J., Blanquart, B., Pobanz, K., Dramais, G., Pierrefeu, G., Hauet, A., Despax, A., 2016. Estimating the uncertainty of streamgauging techniques using in situ collaborative interlaboratory experiments. J. Hydraul. Eng. 142 (7) 04016011.
LeBoursicaud, R., Pénard, L., Hauet, A., Thollet, F., LeCoz, J., 2015. Gauging Extreme Floods on YouTube: Application of LSPIV to Home Movies for the Post-event Determination of Stream Discharges. Hydrological Processes.
Lloyd, P.M., Stansby, P.K., Ball, D.J., 1995. Unsteady surface-velocity field measurement using particle tracking velocimetry. J. Hydraul. Res. 33 (4), 519–534.
Ludovisi, R., Tauro, F., Salvati, R., Khoury, S., Scarascia Mugnozza, G., Harfouche, A., 2017. UAV-based thermal imaging for high-throughput field phenotyping of black poplar response to drought. Front. Plant Sci. 8.
Manfreda, S., McCabe, M.F., Miller, P.E., Lucas, R., Madrigal, V.P., Mallinis, G., Ben Dor, E., Helman, D., Estes, L., Ciraolo, G., Müllerová, J., Tauro, F., De Lima, M.I., De Lima, J.L.M.P., Frances, F., Caylor, K., Kohv, M., Maltese, A., Perks, M., Ruiz-Pérez, G., Su, Z., Vico, G., Toth, B., 2018. On the use of unmanned aerial systems for environmental monitoring. Remote Sens. 10 (4), 641.
Moramarco, T., Saltalippi, C., Singh, V.P., 2004. Estimation of mean velocity in natural channels based on Chiu's velocity distribution equation. J. Hydrol. Eng. 9 (1), 42–50.
Moroni, M., Cushman, J.H., 2001. Three-dimensional particle tracking velocimetry studies of the transition from pore dispersion to Fickian dispersion for homogeneous porous media. Water Resour. Res. 37 (4), 873–884.
Muste, M., Fujita, I., Hauet, A., 2008. Large-scale particle image velocimetry for measurements in riverine environments. Water Resour. Res. 44 (4) W00D19.
Perks, M.T., Russell, A.J., Large, A.R.G., 2016. Technical note: advances in flash flood monitoring using unmanned aerial vehicles (UAVs). Hydrol. Earth Syst. Sci. 20 (10), 4005–4015.
Peterson, S.D., Chuang, H.S., Wereley, S.T., 2008. Three-dimensional particle tracking using micro-particle image velocimetry hardware. Meas. Sci. Technol. 19 (11), 115406.
Radice, A., Sarkar, S., Ballio, F., 2017. Image-based Lagrangian particle tracking in bedload experiments. J. Vis. Exp. 125 e55874.
Raffel, M., Willert, C.E., Wereley, S.T., Kompenhans, J., 2007. Particle Image Velocimetry A Practical Guide. Springer, New York.
Tang, H.W., Chen, C., Chen, H., Huang, J.T., 2008. An improved PTV system for large-scale physical river model. J. Hydrodyn. 20 (6), 669–678.
Tauro, F., Petroselli, A., Porfiri, M., Giandomenico, L., Bernardi, G., Mele, F., Spina, D., Grimaldi, S., 2016. A novel permanent gauge-cam station for surface-flow observations on the Tiber River. Geosci. Instrum. Methods Data Syst. 5 (1), 241–251.
Tauro, F., Piscopia, R., Grimaldi, S., 2017. Streamflow observations from cameras: large-scale particle image velocimetry or particle tracking velocimetry? Water Resour. Res. 53 (12), 10374–10394.
Tauro, F., Porfiri, M., Grimaldi, S., 2014. Orienting the camera and firing lasers to enhance large scale particle image velocimetry for streamflow monitoring. Water Resour. Res. 50 (9), 7470–7483.
Tauro, F., Porfiri, M., Grimaldi, S., 2015. Surface flow measurements from drones. J. Hydrol. 540, 240–245.
Tauro, F., Salvatori, S., 2016. Surface flows from images: ten days of observations from the Tiber River gauge-cam station. Hydrol. Res. 49 (1) Nh2016302.
Tauro, F., Selker, J., vandeGiesen, N., Abrate, T., Uijlenhoet, R., Porfiri, M., Manfreda, S., Caylor, K., Moramarco, T., Benveniste, J., Ciraolo, G., Estes, L., Domeneghetti, A., Perks, M.T., Corbari, C., Rabiei, E., Ravazzani, G., Bogena, H., Harfouche, A., Brocca, L., Maltese, A., Wickert, A., Tarpanelli, A., Good, S., LopezAlcala, J.M., Petroselli, A., Cudennec, C., Blume, T., Hut, R., Grimaldi, S., 2018. Measurements and observations in the XXI century (MOXXI): innovation and multidisciplinarity to sense the hydrological cycle. Hydrol. Sci. J. 63 (2), 169–196.
Uijttewaal, W.S.J., Lehmann, D., vanMazijk, A., 2001. Exchange processes between a river and its groyne fields: model experiments. J. Hydraul. Eng. 127 (11), 928–936.
Wu, Q.X., Pairman, D., 1995. A relaxation labeling technique for computing sea surface velocities from sea surface temperature. IEEE Trans. Geosci. Remote Sens. 33 (1), 216–220.
Yossef, M.F.M., deVriend, H.J., 2011. Flow details near river groynes: experimental investigation. J. Hydraul. Eng. 137 (5), 504–516.